Characterizing the Near-Field Region of a Spray using White Beam and Focused Beam X-ray Measurements

J. K. Bothell[1], D. Li[1], T. B. Morgan[1], T. J. Heindel[1],
A. Aliseda[2], N. Machicoane[2], A. L. Kastengren[3]
[1]Department of Mechanical Engineering, Iowa State University, USA
[2]Department of Mechanical Engineering, University of Washington, USA
[3]X-Ray Science Division, Advanced Photon Source, Argonne National Laboratory, USA

Abstract

A current area of investigation is controlling sprays using real-time feedback. In working towards this goal, it is necessary to create a reduced-order model of the spray. The model will then be used to determine the best method of monitoring the spray, and provide an estimate of the resulting change from the controlling mechanism. The current work focuses on characterizing the near-field region of a coaxial airblast atomizer, to eventually formulate a data-driven model for spray control. High-speed white beam imaging and focused beam X-ray measurements of the near-field region of the atomizer have been recorded at the Advanced Photon Source. We characterize a natural harmonic that starts near the nozzle outlet and progresses to a maximum instability in the near-field region. Liquid ligaments and internal air bubbles are observed in a region that was previously thought to be a continuous liquid core. Swirl has been added to the air stream of the atomizer and has been shown to change the location of maximum instability as well as the shape of the spray. All of these tests resulted in an area of particular interest approximately one to two nozzle diameters downstream from the nozzle outlet, and it is shown that it is the location of primary breakup, pinching spray angle, maximum standard deviation, and maximum instability. Future work will combine the current data with those obtained in the far-field region to create a reduced-order model for spray control.

Keywords: Atomization, drop, high-speed imaging, primary breakup, spray, synchrotron, time-resolved X-ray diagnostics

---

Introduction

Although there are many applications for a controlled spray, engineering difficulties preclude real-time control of most sprays. Before active control will be possible, a reduced-order model of the spray will be necessary. This reduced-order model needs to have a prediction of the spray characteristics at control conditions as well as an estimate of the ways that the spray will change when control mechanisms are used. In using spray control, it will likely not be possible to monitor the entirety of the spray at any point in time, so the model will also provide information about the system that active monitoring will not be able to provide.

To create the reduced-order model for the spray, it first needs to be well characterized at control conditions. Because of the different dynamics in the near-field and far-field region of a spray, different techniques are required to characterize each section. The techniques to characterize the far-field region include, but are not limited to, hotwire anemometry [1], high-speed imaging [2], shadowgraphy [3], phase Doppler anemometry [4], and particle image velocimetry [5]. A combination of these techniques shows droplet size distribution, the droplet velocity field, and gas velocity field. Experimental techniques for the near-field region are extremely limited due to the complex interfaces and high optical density of this region. Ballistic imaging and X-ray measurements have recently shown potential [6, 7] because they can penetrate the area with light and X-rays, respectively. This paper explores new near-field analysis techniques of sprays using synchrotron X-ray measurements. A companion paper explores the use of broadband X-ray imaging to measure spray characteristics [8]. Another companion paper assesses the feasibility of using monochromatic X-ray imaging to characterize sprays [9].

Experimental Methods

This study is using an airblast atomizer as shown in Figure 1a with a simple, well-defined and published geometry [10], making it an ideal candidate as a canonical spray. The nozzle has two concentric tubes, that are in line at the nozzle exit, where there is liquid flow in the inner tube and air flow in the outer tube, shown in Figure 1b. The actual liquid flow inner diameter at the nozzle exit, as measured through X-ray radiographs, is 2.1 mm. The exterior diameter of that liquid nozzle is 2.7 mm. The interior diameter of the gas nozzle at the exit is 10.0 mm.

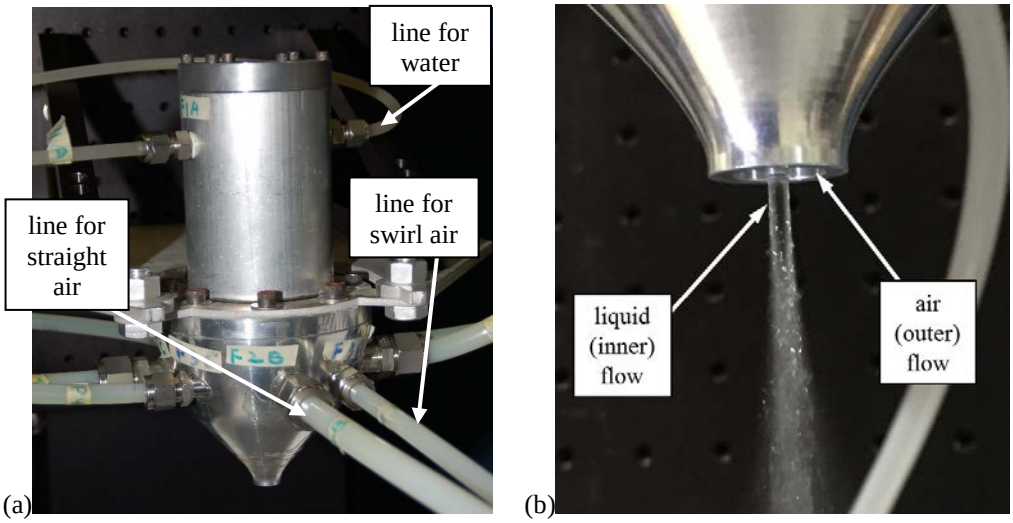

Figure 1: The airblast atomizer used in experiments: (a) the water and air inlets and (b) a close-up of the nozzle exit.

As shown in Figure 2, the nozzle is attached to a two-dimensional translation stage that is capable of moving in the vertical and horizontal directions with a precision of less than 5 µm. This setup makes it possible to image or make measurements at selected flow locations while the X-ray beam remains fixed. The spray is directed downward into a spray catchment system. Mild suction is applied in the exhaust stream to prevent spray recirculation. For reference, the z-direction is defined as the X-ray beam propagation direction, the y direction is axially, and the x-direction is transverse to the spray axis.

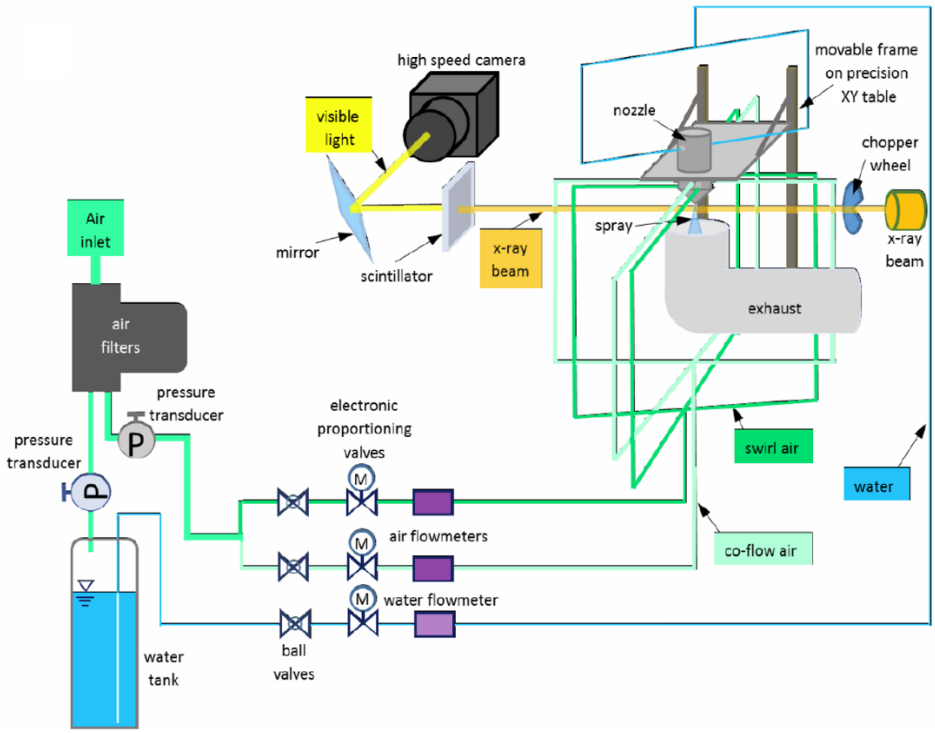

Figure 2: Schematic of the Advanced Photon Source (APS) experimental setup for white beam imaging.

An 18.9 liter tank, pressurized with air, supplies distilled water to the nozzle, as shown in Figure 2. An electronic proportioning valve is used to control the flow rate and a water flow meter monitors the instantaneous flow rate and cumulative volume. Air for the injectors is filtered and partitioned into two systems for main and swirl air. Electronic proportioning valves and air flow meters control and monitor the air flow rates.

The electronic proportioning valves and flow meters are all connected to a data acquisition system that provides real-time measurement and control. The electronic proportioning valves are controlled by a PID (Proportional, Integral, and Derivative) active control system that was built in LabVIEW. Values from the flow

meters are used as the feedback to drive the PID system. The LabVIEW program also stores all flow data so that it can be correlated to any phenomenon that is seen in the flow.

It should be noted that an identical flow system from the liquid and gas flow meters to the nozzle exit, including an identical nozzle, is used in a separate facility investigating far-field spray characteristics [10]. This ensures identical flow conditions can be recreated in both flow systems.

The camera used for high-speed imaging at APS is a Photron FASTCAM Mini AX50 camera with a 105 mm and 50 mm lens combination, providing an effective magnification of 2.01. The image capture rate varies between 6 and 13.6 kHz, where the faster capture rates are used for the higher liquid and gas flow rates. The camera is shielded with a leaded bronze case to minimize the potential damage from radiation.

The X-ray beam is set up for two types of measurements: full-field imaging with the polychromatic white beam, and focused beam measurements with a monochromatic X-ray beam. Focused beam measurements are best for quantitative analysis because of the high accuracy and time resolution, whereas white beam imaging is better for qualitative analysis of the spray because it provides images with a larger field of view but less accuracy in determining the effective path length.

For white beam imaging, the beam enters the hutch that contains the experimental setup (Figure 2) through a 250 μm thick beryllium window, after which there is a rotating chopper wheel that blocks the beam periodically to reduce heat loading on the experimental equipment. After passing through the chopper wheel, the beam passes through the nozzle spray, decreasing in intensity dependent on the effective path length of liquid. It is then captured by a scintillator crystal (500 μm thick YAG:Ce (Cerium doped Yttrium Aluminum Garnet)) that emits visible light proportional to the X-ray intensity. The visible light is reflected off of a dichroic mirror and into the lens of the camera. The images are 3.0 mm by 2.5 mm, have a resolution of 608 × 512 pixels, and were taken at an exposure of 1.05 μs. When using the white beam setup, the imaging area that is available allows for radiographs that can be stitched together to cover the entire region of interest [11].

For the focused beam measurements, a monochromator and focusing mirrors are added to the setup and the chopper wheel is not used. Because the beam is focused to such a small region (5 by 6 μm), data are taken by raster scanning across the spray at several (x,y) locations. A PIN photodiode is used to record the X-ray intensity as a function of time. These measurements are taken at 6.25 MHz for 10 seconds. The energy of the monochromatic beam is 8 keV. The signal error for focused beam measurements, calculated as the average standard deviation of the beam intensity with no signal is 9.75×10^{-5} mm.

Results and Discussion

White beam imaging is necessary to visualize the region and see a larger field of view. However, more accurate, more highly time-resolved results come from focused beam measurements. The PIN diode measures the intensity of a monochromatic beam after passing through the liquid that is in that region, at that time. The use of a narrow band (4% ΔE/E) of X-ray wavelengths allows the use of a simplified version of Beer-Lambert's law:

$$\ell = \frac{1}{\mu}\ln\left(\frac{I_0}{I}\right) \tag{1}$$

where ℓ is the effective path length (EPL) defined as the path length-integrated quantity of liquid in the X-ray beam, I_0 is the intensity of the incident beam, I is the intensity at the PIN diode after the beam passes through the spray, and μ is the X-ray attenuation coefficient. I_0 is measured in the region outside of the spray, and all measurements are taken in a highly time-resolved fashion. This provides a highly time-resolved measurement of EPL vs. time.

Flow conditions are defined by the liquid Reynolds number (Re_l), gas Reynolds number (Re_g), and the swirl ratio (SR). The flow conditions for this study use a liquid Reynolds number Re_l = 1,000, as defined by

$$Re_l = \frac{U_{m,l} D_i}{\nu_l} \tag{2}$$

where $U_{m,l}$ is the mean liquid velocity ($U_{m,l} = Q_l/Area_l$), D_i is the inner diameter of the liquid nozzle, and ν_l is the liquid kinematic viscosity. The gas Reynolds number Re_g = 16,700 for all conditions is defined by

$$Re_g = \frac{U_{m,g} D_h}{\nu_g} \tag{3}$$

where $U_{m,g}$ is the mean gas velocity ($U_{m,g} = Q_g/Area_l$), D_h is the hydraulic diameter, and ν_g is the gas kinematic viscosity. For concentric tubes like the nozzle exit in this study, the hydraulic diameter is simply $D_{g,o}$ - $D_{g,i}$, which is the difference between the outer and inner diameter of the annular gas nozzle. The swirl ratio varies for different conditions and is defined by

$$\text{SR} = \frac{\text{tangential gas flow rate}}{\text{parallel gas flow rate}} \tag{4}$$

A comparison of three types of data that are all obtained from focus beam measurements is shown in Figure 3. Figure 3a is a short clip of the path length over time that contains 2500 data points from a set that is 6 million data points in total. The path length is computed from the intensity as a function of time measurements using Eq. (1). Figure 3b shows the average path length and is calculated by averaging the path length data from each data point and then linearly interpolating between those points to obtain the entire flow field. Figure 3c is a map of standard deviation values that was created by calculating the standard deviation at each point and linearly interpolating between those points to estimate the entire flow field.

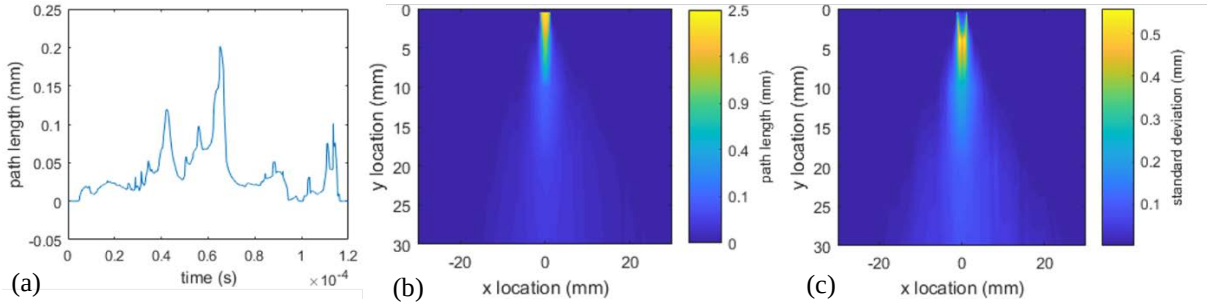

Figure 3: Data available from focused beam measurements with Re_l = 1,000, Re_g = 16,700, and SR = 0 (a) short clip of path length as a function of time, taken from x=0, y=4 (b) average path length (c) path length standard deviation.

When compared to focused beam imaging, white beam imaging can show a much larger field of view than focused beam measurements but cannot show the entire flow field at once. Because of this, the area must be imaged in sections. Figure 4a shows the locations of instantaneous imaging regions against a map of time-averaged liquid path length calculated from the focused beam measurements; average focused beam measurements are linearly interpolated between data points where no data were taken. Since the instantaneous imaging is done in sections, it is not always possible to tell what was happening upstream that caused an instantaneous shape or structure to take form. In the same way, it is difficult to predict how the spray will progress from any given frame or series of images.

In Figure 4b many liquid ligaments can be seen and are a prominent feature at this downstream location. As the flow progresses those ligaments begin breaking apart to form droplets. The overall number of ligaments decreases as the flow progresses, with droplets becoming the more dominant feature.

Figure 4c was taken from higher in the flow but at the same flow condition as the first image. The liquid here is thick and just beginning to break up. Air bubbles are common in this region and often are trapped at a location for a short period of time whereas droplets constantly move away from the nozzle as would be expected.

Figure 4d was taken at the same liquid and gas flow rate (Re_l = 1,000 and Re_g = 16,700) but with a swirl ratio SR = 1. This image was chosen because of the multiple bags that can be seen at the same time. The two bags on the right have just formed and as they progress will break apart into droplets. Along the left side, a bag that had formed earlier in the spray and is in the middle of breaking apart into droplets can be seen.

A combination of these two techniques can be seen in Figure 5 which were taken at flow conditions Re_l = 1,000, Re_g = 16,700, and SR = 0. Figure 5a is a map of the standard deviation of the EPL, taken from focused beam raster scan measurements and the values between the point measurements were estimated by linear interpolation. Figure 5b is an instantaneous white beam image that was taken from the location as indicated by the red box on the standard deviation chart. The imaging area covers the region where the standard deviation is the highest. From this image, the beginning of droplet formation is shown. This location is the closest to the nozzle where the formation of individual droplets are typically observed.

The location of primary breakup is a topic of interest and is a difficult parameter to define. In this study, the uppermost location of droplets breaking off the liquid core (as seen in X-ray imaging) was compared to the location of maximum standard deviation. Figure 5 is an example of these comparisons. In all the locations that were tested, the region over which droplets began to form corresponded with the region showing the maximum standard deviation. Hence, the bright yellow region in Figure 5 can be defined as the primary breakup region.

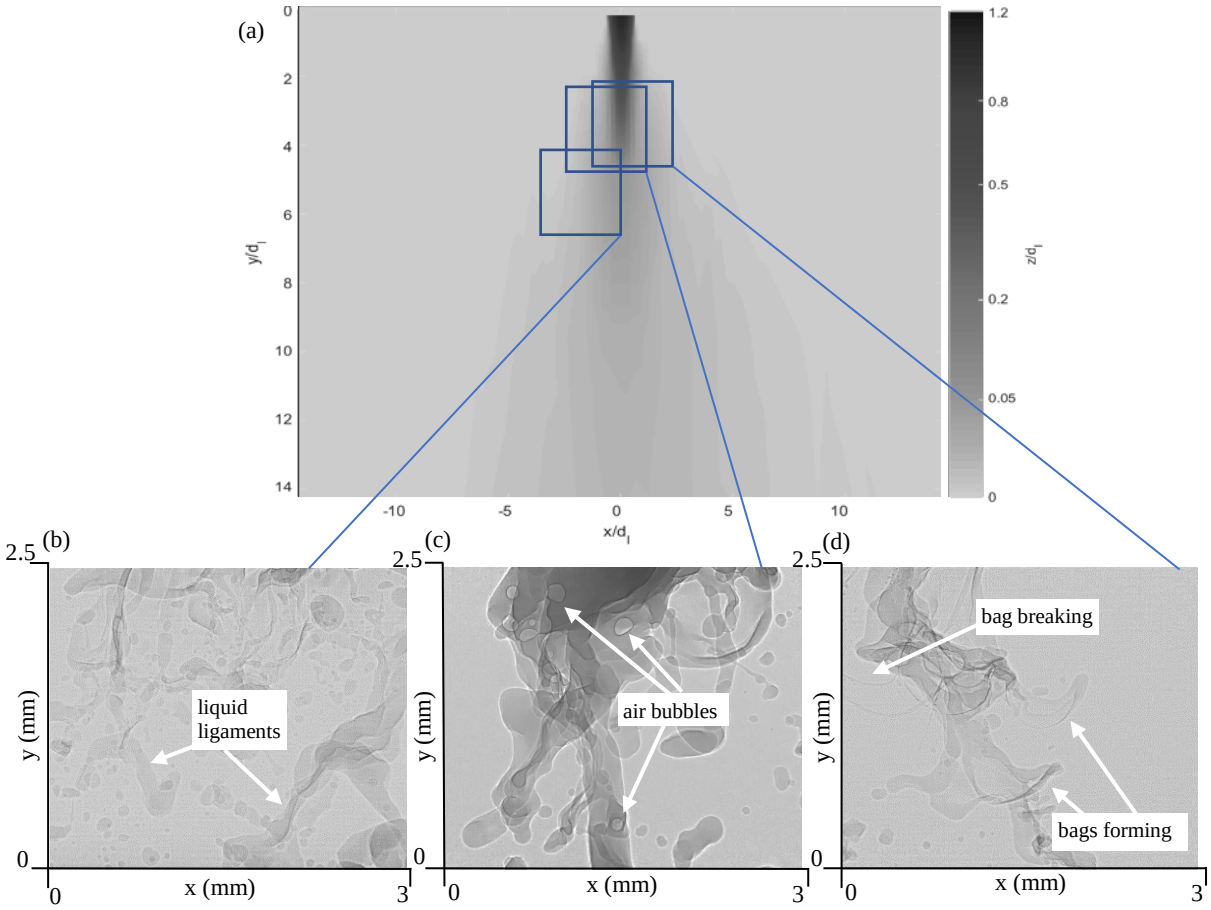

Figure 4: Spray dynamics in the near-field region against an average flow field: (a) average flow field, (b) liquid ligaments, (c) air bubbles, and (d) bags forming and breaking.

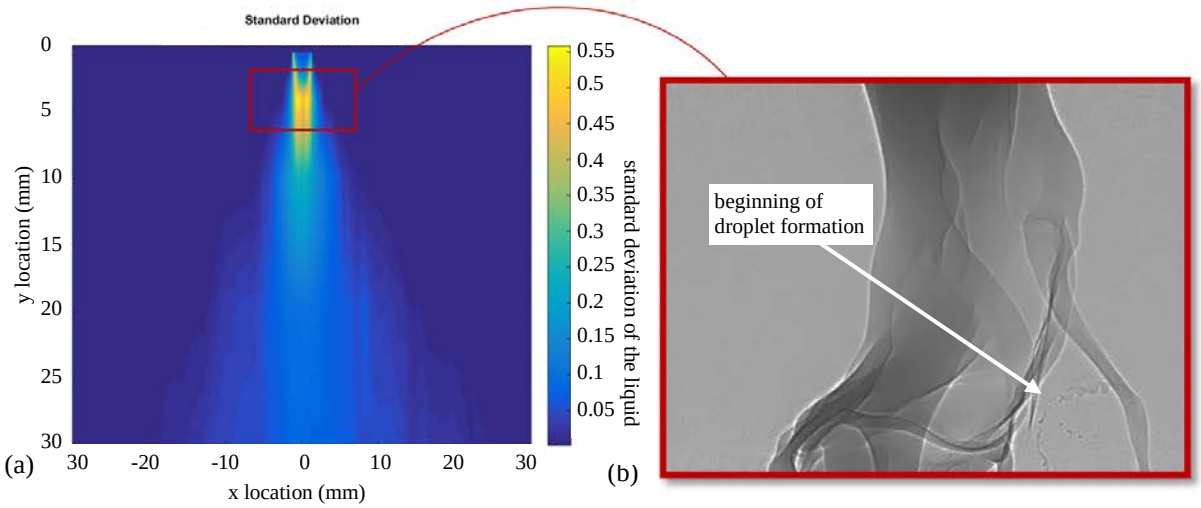

Figure 5: A comparison of (a) the maximum standard deviation to (b) white beam image for Re_l = 1,000, Re_g = 16,700, and SR = 0.

Changing the air flow swirl ratio influences the instantaneous shapes that are seen, as shown in Figure 4, but it also changes the average shape of the spray. Using focused beam measurements, the average path length along each of the raster scans was calculated. Fitting a curve to the raster scan, the effective path length was determined to be Gaussian from very near the nozzle, as shown in Figure 6. From the Gaussian distribution, the maximum path length along each scan was used as the center line of the spray. The spray edge location was calculated by defining the edge of the spray as the location of 50% of the maximum or ½ EPL_{max} as shown in Figure 6a . Shown in Figure 6b are three spray edges with the same total flow rates (Re_l = 1,000 and Re_g = 16,700) but with differing

swirl ratios. In each of these conditions, there is a y-location where the spray is the narrowest, which will be referred to as the pinching location. This pinching location is around 4 mm for the condition with no swirl, SR = 0, around 2 mm for the condition with SR = 0.5 and around 4 mm for the condition with SR = 1. The exact location of the pinching cannot be determined with the current data because the raster scans resulted with a coarse grid in the vertical direction. It is also worth noting that the spray with the widest angle shows up at SR = 0.5, and both the higher and lower swirl ratios in this study result in a more narrow spray.

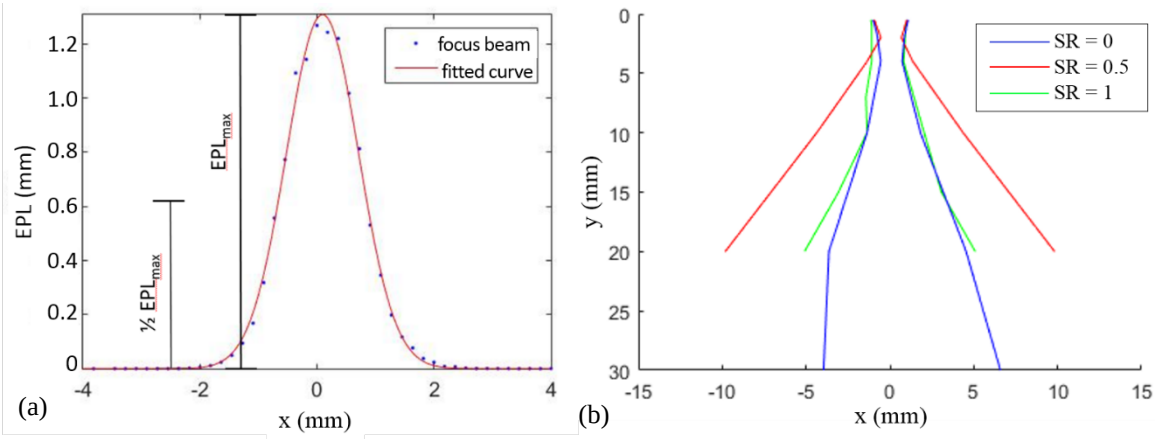

Figure 6: Defining and comparing spray angles for the spray at the flow condition Re_l = 1,000 and Re_g = 16,700: (a) Defining ½ EPL_{max} (b) Pinching location moves closer to the nozzle for SR = 0.5 and the spray angle is the largest at this flow condition.

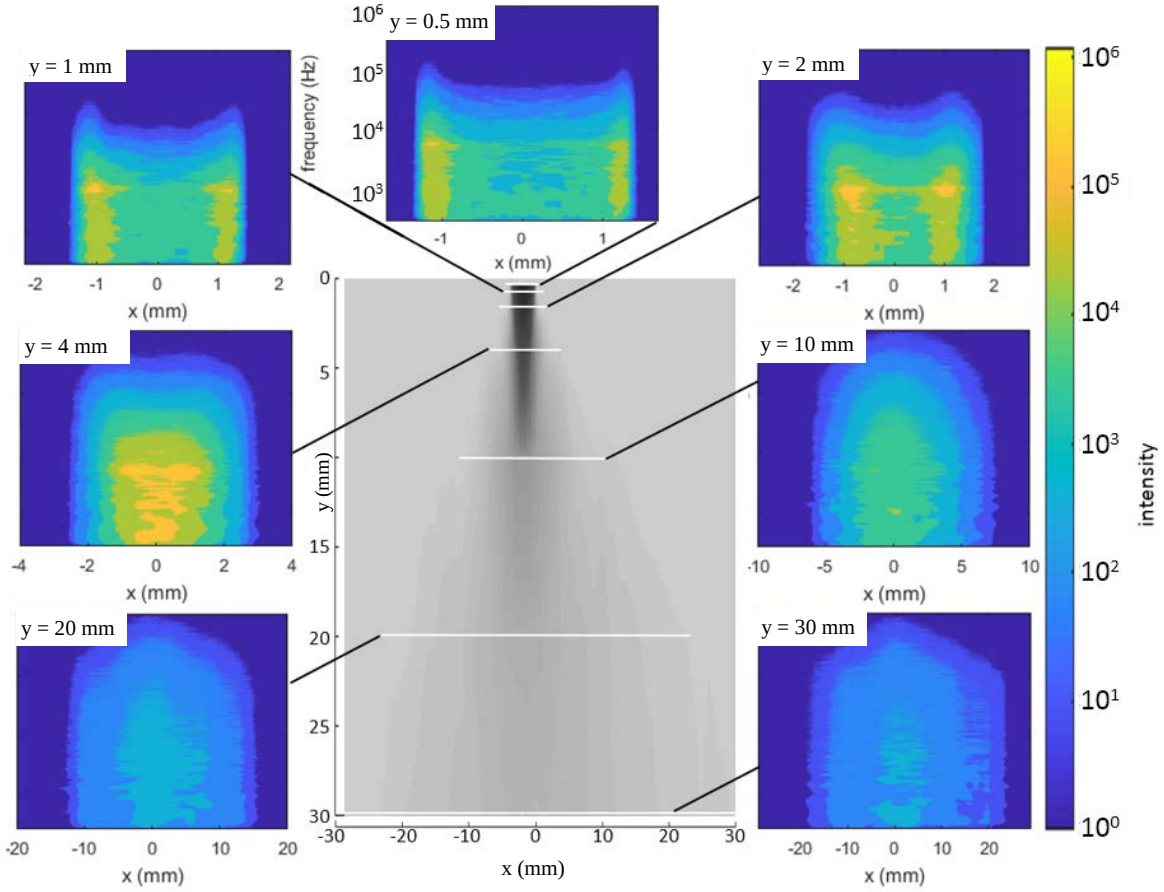

Figure 7: Frequency plots from focused beam raster scans with Re_l = 1,000, Re_g = 16,700, and SR = 0.

The focused beam measurements were also used to determine the frequencies that are present across each of the scans. Figure 7 shows frequency plots for those scans. The bottom center image in Figure 7 is an average flow field for the condition Re_l = 1,000, Re_g = 16,700, and SR = 0. The horizontal lines across the center image

represent the downstream location at which the focused beam scan was completed (this is also shown by the given y-location on each spatio-spectral plot) and the length of the line represents the span of the scan. The frequency scale for all of the frequency plots is the same scale as shown along the left side of the top image and the intensity scale for the power spectra is along the right side of the figure.

The first frequency plot in Figure 7, taken at 0.5 mm down from the nozzle exit, shows a dominant frequency of just below 10 kHz that originates along the edges of the liquid stream. The inner diameter of the nozzle is 2.1 mm and the instabilities are shown to go slightly beyond that. From there, the intensity of the frequencies increases as the flow progresses to around 2-4 mm but decreases as the flow moves past 4 mm. Around 2 and 4 mm, the third and fourth scan down, is the location with maximum fluctuation intensity which could be linked to a maximum instability. These high-intensity frequencies show that there is a range of natural harmonics. The harmonic with a consistently high intensity occurs just below 10 kHz. The region around 2-4 mm was shown in Figure 5 as the region where the standard deviation is the highest and primary breakup occurs. Hence, the region of maximum high frequency fluctuations occurs near the maximum standard deviation, which also corresponds to the pinching location identified in Figure 6. As the flow progresses even further downstream, the high frequencies shift toward the center of the spray and become much less intense.

Figure 8 shows what happens when the swirl ratio is increased to SR = 1 (Re_l = 1,000, Re_g = 16,700, and SR = 1). It is similar to the condition shown in Figure 7 in that the scan closest to the nozzle shows a dominate frequency along the edges of the liquid stream. As the flow progresses, the frequencies increase around 4 mm downstream and then decrease. The highest intensities move from the outer edge toward the center as the flow moves away from the nozzle. All of this is similar to the condition with no swirl. However, in the condition with swirl, the high intensities move toward the center closer to the nozzle. Also, the overall highest intensity isn't seen until approximately 4 mm downstream. The spike that is seen just below 100,000 Hz is much less prevalent when there is no swirl.

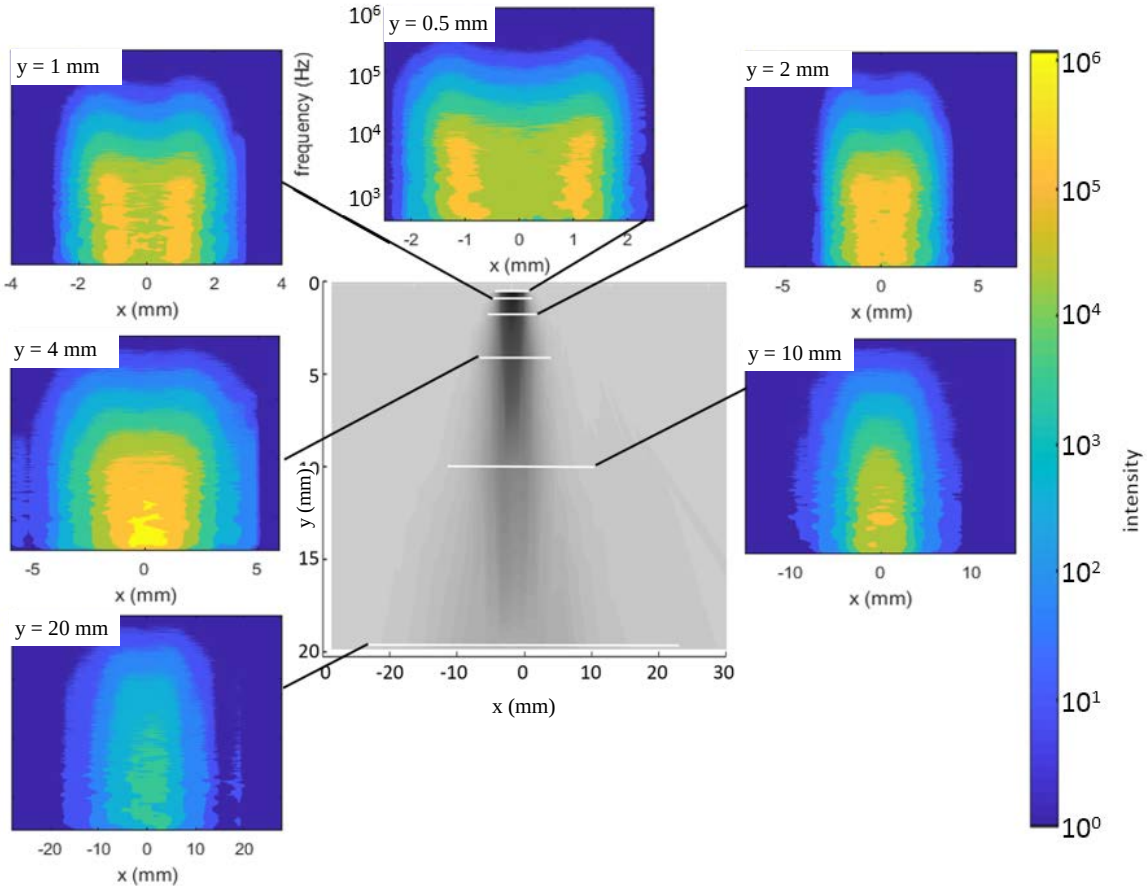

Figure 8: Frequency plots for focused beam raster scans with Re_l = 1,000, Re_g = 16,700, and SR = 1.

Comparing the data from the conditions shown in Figures 7 and 8 to white beam imaging, the regions where there are high intensities on both sides of the jet axis is when a liquid core is still intact. As that begins to merge toward the center, the liquid core is quickly breaking apart. Further downstream, the intensities decrease, and from white beam imaging, it is seen that this region is mostly droplets.

Conclusions

White beam and focused beam X-ray imaging were completed on a canonical airblast atomizer at Re_l = 1,000, Re_g = 16,700, and SR = 0, 0.5, and 1. It was shown that the region 2-4 mm down from the nozzle outlet (approximately one to two nozzle diameters down) was where primary breakup, the spray angle pinch location, and maximum instabilities all were found.

Instantaneous, high-speed white beam imaging allowed for interesting atomization structures to be visualized, including bags, ligaments, droplets, and bubbles inside the liquid. These images also showed that liquid breakup for these flow conditions was typically in the 2-4 mm region from the nozzle exit. Comparing plots of the focused beam standard deviation to white beam images, it was found that the region where the standard deviation is the highest was also the region of primary breakup. The spray angle was shown to have a pinching point around 2-4 mm, depending on the flow conditions. It was also shown that a swirl ratio of SR = 0.5 resulted in the largest spray angle and pinching point closest to the nozzle exit. Frequency plots showed instabilities on the sides of the spray, near the nozzle, that progress to a maximum instability around the 2-4 mm location.

Moving forward, these results will be used to help create a reduced-order model, with the ultimate goal of creating an active flow control spray system.

Acknowledgments

This work was sponsored by the Office of Naval Research (ONR) as part of the Multidisciplinary University Research Initiatives (MURI) Program, under grant number N00014-16-1-2617. The views and conclusions contained herein are those of the authors only and should not be interpreted as representing those of ONR, the U.S. Navy or the U.S. Government.

This work was performed at the 7-BM beamline of the Advanced Photon Source, a U.S. Department of Energy (DOE) Office of Science User Facility operated for the DOE Office of Science by Argonne National Laboratory under Contract No. DE-AC02-06CH11357.

References

[1] Liu, H., “Measurement techniques for droplet properties and intelligent control of droplet processes,” *Science and Engineering of Droplets*, pp. 397–450, 1999.

[2] Marmottant, P., Villermaux, E., “On spray formation,” *Journal of Fluid Mechanics*, 498, 73-111, 2004.

[3] Castrejón-García, R., Castrejón-Pita, J. R., Martin, G. D., and Hutchings, I. M., "The shadowgraph imaging technique and its modern application to fluid jets and drops," *Revista Mexicana de Fisica* 57-3; pp. 266–275, 2011.

[4] Ofner, B., "Phase doppler anemometry," *Optical Measurements: Techniques and Applications*, Springer, pp. 139–152, 1993.

[5] Raffel, M., Willert, C. E., and Kompenhans, J., *Particle Image Velocimetry: A Practical Guide*., Springer, 1998.

[6] Linne, M. A., Paciaroni, M., Berrocal, E., and Sedarsky, D., "Ballistic imaging of liquid breakup processes in dense sprays," *Proceedings of the Combustion Institute*, 32 II(2); pp. 2147–2161, 2009.

[7] Duke, D. J., Kastengren, a. L., Tilocco, F. Z., and Powell, C. F., "Synchrotron X-ray measurements of cavitation," in *ILASS-Americas 25th Annual Conference on Liquid Atomization and Spray Systems*, Pittsburg, PA, May 2013.

[8] Li, D., Bothell, J. K., Morgan, T. B., Heindel, T. J., Aliseda, A., Machicoane, N., Kastengren, A. L., "Quantitative analysis of an airblast atomizer near-field region using broadband and narrowband X-ray sources," in *ICLASS 2018, 14th Triennial International Conference on Liquid Atomization and Spray Systems*, Chicago, Illinois, July 22-26, 2018.

[9] Morgan, T. B., Bothell, J. K., D. Li, Heindel, T. J., Aliseda, A., Machicoane, N., Kastengren, A. L., "Feasibility of monochromatic Xray imaging of the near-field region of an airblast atomizer," in *ICLASS 2018, 14th Triennial International Conference on Liquid Atomization and Spray Systems*, Chicago, Illinois, July 22-26, 2018.

[10] Machicoane, N., and Aliseda, A., "Experimental characterization of a canonical coaxial gas-liquid atomizer," in *ILASS - Americas 2017: 29th Annual Conference on Liquid Atomization and Spray Systems, Atlanta, GA*, May 15-18, 2017.

[11] Kastengren, A., Powell, C. F., Arms, D., and Dufresne, E. M., "The 7BM beamline at the APS: A facility for time-resolved fluid dynamics measurements," *Journal of Synchrotron Radiation*, 19: pp. 654–657, 2012.